Final technical report for USGS EHP award no. G17AP00016
"Models for aseismic fault slip in response to fluid injection"
1 Jan. 2017 – 31 Dec. 2017

PI: Robert C. Viesca*
Tufts University, Medford, MA 02155

Abstract

The occurrence of induced seismicity has been tied to fluid injection into deep, permeable, subsurface layers associated with the extraction of both renewable and non-renewable sources of energy (*Ellsworth*, 2013). The occurrence of these earthquakes have mostly been tied to the subsurface migration of injection-induced elevated pore-fluid pressures, or associated poroelastic stresses, onto tectonically pre-stressed faults thus destabilizing them. In our funded proposal, we had proposed to study a mechanism which might act in parallel to these processes in triggering the seismicity observed in response to subsurface fluid-injection: fluid-activated aseismic slip.

While there is accumulating evidence for the ubiquitous occurrence of fluid-induced aseismic slip across different tectonic regimes, its probable role in triggering induced seismicity, especially on faults which lie beyond the fluid-pressurized region, remains little studied. We report here results from our study that combined theoretical and numerical analysis of fluid-activated aseismic shear ruptures, and assimilated *in situ* continuous measurements of pore-pressure and fault slip from field-scale fluid-injection experiments, to provide a data-derived prediction of fault behavior under these conditions. In our model, we coupled axi-symmetric pore-pressure diffusion away from the borehole (within a permeable and compliant fault damage zone) to the slip response of a quasi-circular shear rupture governed by a frictional strength criterion. The resultant model provides *in situ* constraints on the hydrological and mechanical properties of the fault and its surrounding medium and the ambient state of stress. We find evidence for permeability enhancement of about 60% with accumulating pore-pressure and slip. The resultant model captures the pore-pressure evolution well with hydrological parameters that are consistent with laboratory-derived values. We further find that the phases of accelerating aseismic slip observed in these experiments cannot be modeled with a shear rupture whose strength is determined by a constant friction coefficient. This provides direct *in situ* evidence that laboratory-derived fault friction relations that allow the friction coefficient to vary with slip and/or slip-rate are necessary to capture 'real' fault behavior. As a proof-of-concept we show that a model that allows the friction coefficient to undergo step-changes with slip rate—a numerically less expensive proxy for slip- or rate-dependence—fits the slip history well. In this sense, besides illuminating our mechanistic understanding of fluid-induced aseismic slip, our study also bridges the gap between our laboratory-derived understanding of fault mechanics and field-scale observations of fault behavior, a crucial step towards building more realistic models of fault operation and earthquake hazard.

*robert.viesca@tufts.edu, phone: +1-617-627-5165, fax: +1-617-627-3994

Publications and presentations funded by this award

Bhattacharya, P., and R. C. Viesca (2017), *Data-driven fault mechanics: Inferring fault hydro-mechanical properties from in situ observations of injection-induced aseismic slip*, Abstract S43C-0876, presented at 2017 Fall Meeting, AGU, New Orleans, LA, 11-15 Dec.

Technical Report

Motivation for modeling the *Guglielmi et al.* (2015a) observations

Fluid-injection into permeable subsurface layers – related to geothermal or oil and gas operations – has been associated with enhanced local seismicity rates in many parts of North America and Europe (*Ellsworth*, 2013; *Weingarten et al.*, 2015; *Keranen et al.*, 2014; *Charléty et al.*, 2007; *Deichmann and Giardini*, 2009). Though usually small in magnitude, the recent occurrence of some large, damaging, induced earthquakes in the U.S. mid-continent has forced the scientific community to re-evaluate the hazard posed by such fluid-injection activities (*Weingarten et al.*, 2015). These earthquakes are widely believed to be triggered by migrating, elevated, pore-fluid pressures which can reduce the effective normal stress on tectonically loaded faults and make them conducive to shear-failure (*Hubbert and Rubey*, 1959; *Raleigh et al.*, 1976; *Ellsworth*, 2013). But fluid-pressurized faults do not always fail with unstable, dynamic slip characteristic of earthquakes. Observed mismatches between total inferred slip and maximum earthquake size on fluid-pressurized faults have been used to suggest that subsurface fluid-injection can also stimulate slow, aseismic slip (*Scotti and Cornet*, 1994; *Cornet et al.*, 1997; *Guglielmi et al.*, 2015a; *Wei et al.*, 2015). In some cases, these fluid-induced aseismic ruptures have been observed to be equivalent to $\mathrm{M} \sim 5$ earthquakes in terms of moment released (*Cornet et al.*, 1997; *Wei et al.*, 2015; *Cornet*, 2016) and, in one such instance (*Wei et al.*, 2015), have been inferred to possibly trigger $\mathrm{M} > 5$ earthquakes at unexpectedly large space and time offsets from injection activity. However, despite this apparent hazard potential associated with fluid-induced aseismic slip, we understand little about the conditions under which fluid-induced aseismic slip occurs in nature, the hydro-mechanical evolution of such ruptures with continued injection and their relationship with fluid-induced earthquakes.

While models based on laboratory-derived frictional constitutive relations do predict that fluid pressurized faults might undergo stable aseismic slip under certain conditions (*Garagash and Germanovich*, 2012), the extent to which these models represent 'real' fault behavior has never been tested owing to the absence of continuous in situ measurements of a fault's evolving hydro-mechanical response with slip. Recent fluid-injection experiments on shallow crustal faults have finally bridged this data gap by activating and measuring fluid induced aseismic slip and pore-pressure evolution in situ (*Guglielmi et al.*, 2015a). One important observation of the *Guglielmi et al.* (2015a) experiments was that fluid injection primarily activated aseismic slip which in turn triggered micro-seismicity as a secondary effect. Besides providing insights into the conditions under which aseismic slip is activated by fluid-pressurization on natural faults, such data could also provide key information about the interaction of aseismic and seismic slip in active fault zones. Even beyond the immediate purview injection-induced seismicity, earthquake triggering by aseismic slip might be a universal feature of fluid rich fault zones and has previously been linked to foreshock production along plate boundaries (*Dodge et al.*, 1996; *Bouchon et al.*, 2013). A sound, observationally constrained, mechanistic understanding of this problem could have important implications for development of realistic numerical models of seismic hazard.

In addition to numerically modeling the *Guglielmi et al.* (2015a) data, we also use these data within a rigorous Bayesian inversion framework to obtain formal constraints on the hydro-mechanical parameters of these models. While the estimate of *in situ* hydrological properties of seismically active faults are not uncommon (*Coyle and Zoback*, 1988; *Shapiro et al.*, 1997, 2002; *Doan et al.*, 2006; *Xue et al.*, 2013), estimates of hydrological properties of faults during and within zones of active slip are rare (*Guglielmi et al.*, 2015b). The evolution of hydraulic properties with slip, in particular permeability enhancement accompanying pore-pressure increase and slip accumulation also provide important constraints on estimates of crustal strength at seismogenic depths (*Townend and Zoback*, 2000). Furthermore, the *Guglielmi et al.* (2015a) dataset also provides unique *in situ* constraints on our almost exclusively laboratory-derived understanding of fault strength evolution with slip and/or slip rate *Dieterich* (1972); *Ruina* (1983); *Marone* (1998); *Marone and Saffer* (2015), in particular in the presence of fluids, the latter remain poorly understood even in the laboratory (*Beeler*, 2007).

In recent years, there has been a growing interest from within diverse cross-sections of the fault-hydrology/seismology communities to set up more such 'natural earthquake laboratories' by carrying out controlled fluid-injection at well-instrumented fault sites. For example, the USGS partially funded a workshop on Scientific Exploration of Induced SeisMicity and Stress (SEISMS) organized at the Lamont-Doherty Earth Observatory in March, 2017 to discuss possible sites, scientific goals and strategies for such a cross-disciplinary, multi-institute, collaborative project. In this context, our study seems like a timely proof of concept in favor of the utility of the derived data and while also providing insights into what additional data could help us impose better constraints.

Model set up

Our model has two components: (i) a hydrologic model assuming axisymmetric fluid flow to determine pore-pressure distributions in response to the imposed injection history (Figure 1A) and (ii) a model for fault slip that assumes uniform pre-injection stress state, a planar fault, and a frictional strength criterion (Figure 1B).

With the assumption that the fault damage zone is orders of magnitude more permeable and compliant than the host rock (from Figure 1A, $k \gg k_o$, $G_o \gg G$), we model fluid flow as fault-parallel and radially outward from the borehole and entirely contained within the fault damage zone acting as a conduit of vertical width b. We consider a cylindrical geometry (r, θ, z) with displacements and pore-pressure $p(r,t)$ as purely radial functions. Since all (purely radially varying) displacements vanish within the effectively rigid host rock, no poro-elastic strains can develop within the damage zone if one additionally assumes that the interfaces between the host rock and the damage zone remain perfectly bonded. Under these conditions, the mass conservation of the fluid in the cylindrical region internally bounded by the borehole of radius r_0 takes the form (*Detournay and Cheng*, 1993):

$$\frac{\partial p}{\partial t} = c\nabla^2 p, \tag{1}$$

where the diffusivity $c = k\rho g/\mu S_s$, μ is the dynamic viscosity of the relevant fluid (Pa·s), ρ its density (kg/m^3), g is acceleration due to gravity (9.81 m^2/s) and S_s is the specific storage (m^{-1}). In the absence of volumetric strains, the specific storage can be identified as inversely proportional to the poro-elastic Biot modulus M (Pa), defined as the increase of the amount of fluid (per unit volume of rock) due to a unit increase of pore pressure, under constant volumetric strain (*Detournay and Cheng*, 1993). Equation (1) is solved on a logarithmic grid with a stiff,

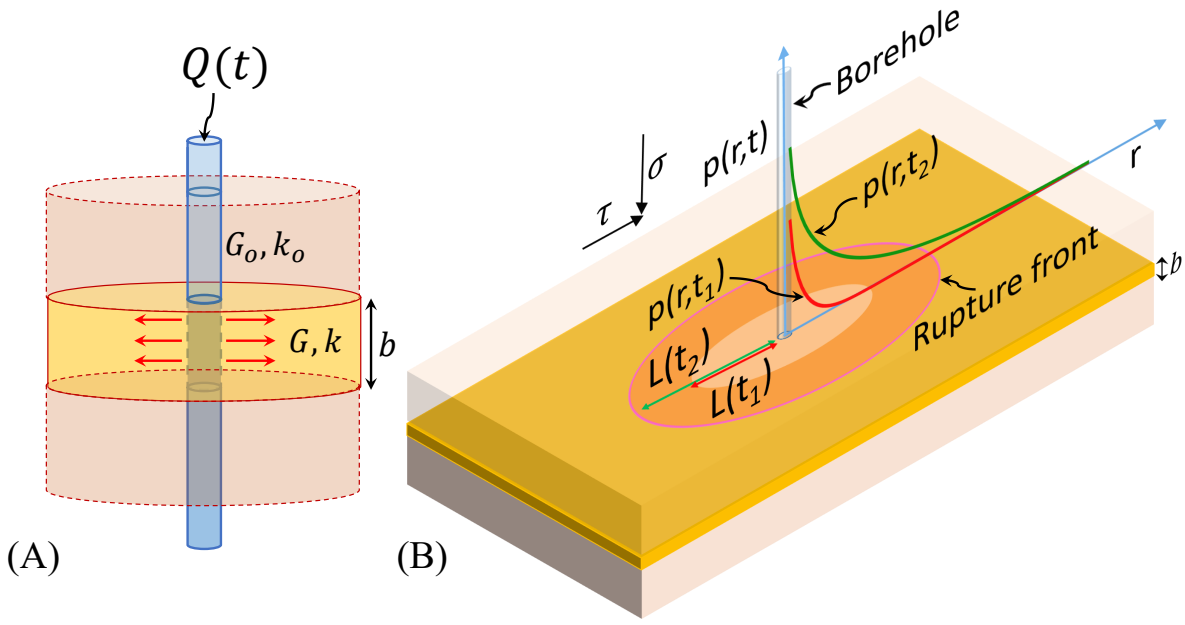

Figure 1: Schematics for the model set up: (A) Axisymmetric pore fluid flow problem presuming injection at the instantaneous volume rate $Q(t)$ through a well of finite radius r_0 into a permeable layer of width b. Pore-pressure is assumed to diffuse through a permeable pathway (thought to be a fault-bounding damage zone) characterized by permeability k and elastic modulus G. This permeable layer is embedded within the host rock characterized by k_o and G_o. We make simplifying assumptions $k \gg k_o$ and $G \ll G_o$ to reduce the full poroelastic problem to one of axisymmetric fluid diffusion through a non-leaky medium. (B) A nearly circular rupture is driven by an increasing pore-fluid pressure distribution which reduces the effective normal stress $\sigma_{\text{eff}} = \sigma - p(r,t)$ where σ is fault resolved normal stress. Assuming $L(t) \gg b$, we model quasi-static slip as occurring within a rupture on the planar interface between two identical elastic half-spaces with modulus G_o. Given a background fault-resolved shear traction τ, the radial diffusion of pore-pressure away from the well with time causes reduction in frictional strength over an increasingly larger area, which in turn allows the rupture to grow.

adaptive time stepping code subject to the variable injection rate imposed at the well. We use an adaptive Markov Chain Monte Carlo code to obtain the full posteriors for k and M by fitting the pore-pressure data of *Guglielmi et al.* (2015a).

From our numerical fits to the pore-pressure data, we obtain the spatio-temporal distribution of pressure $p(r,t)$ for the imposed time-history of injection. With time, this radially outward pore-pressure diffusion reduces the effective normal stress $\sigma_{\text{eff}} = \sigma - p(r,t)$ over progressively larger regions. This reduction in σ_{eff} leads to a reduction in frictional resistance to sliding (expressed as the product of a constant friction coefficient and σ_{eff}), and in the presence of a background fault-resolved shear traction τ, which drives the growth of a circular rupture of instantaneous radius $L(t)$ (Figure 2B). For rupture dimension $L(t) \gg b$, the shear rupture has no sensitivity to the elastic modulus of the permeable layer and one can write the quasi-static force balance as (*Salamon and Dundurs*, 1971, 1977):

$$f[\sigma - P(r,t)] - \tau = -\frac{G_o}{2\pi}\int_0^{L(t)} \frac{\partial}{\partial s}\delta(s,t)\left[\frac{1}{s-r}E\left\{k\left(\frac{r}{s}\right)\right\} + \frac{1}{s+r}F\left\{k\left(\frac{r}{s}\right)\right\}\right] ds, \quad (2)$$

where f is the friction coefficient, $\delta(r,t)$ is the instantaneous slip profile and E,F are the complete elliptic integrals of 2nd and 1st kinds and $k(U) = 2\sqrt{U}/(1+U)$. This assumes an axisymmetric, circular rupture of radius $L(t)$, which is expected only if the Poisson ratio $\nu = 0$. However, a small correction (*Gao*, 1988) permits us to use this solution to accurately represent the general case where $\nu \neq 0$. One can solve the integral equation in Equation (2) for the equilibrium slip profile $\delta(r,t)$ and the instantaneous rupture radius $L(t)$ given a particular choice of G_{out}/f and $1-\tau/f\sigma$. We use an efficient (implying high accuracy for small number of grid points) Chebyshev scheme to invert for $\delta(r,t)$ and $L(t)$ with a Newton-Raphson scheme. We then use the predicted value of $\delta(r_0,t)$ to fit the observed slip at the well which allows us to infer the appropriate values of G/f and $1-\tau/f\sigma$.

Inversion methodology

For all our inversions, we use a Markov Chain Monte Carlo algorithm to infer the parameter posteriors in a Bayesian sense. We use an adaptive proposal – small world Metropolis-Hastings strategy for this purpose (*Bhattacharya et al.*, 2015), the code is freely available at `https://github.com/pathikrit-bhattacharya/MCMC_fortran_library`.

The code uses Metropolis-Hastings (*Metropolis et al.*, 1953; *Hastings*, 1970) sampling to construct an approximate Markov chain of accepted parameters which sample the joint posterior distribution of the parameters given the data. The prior distribution was generally assumed to be uniform (i.e., a non-informative prior). Given the observed data vector and the modeled data vector, we use different norms (both ℓ_1 and ℓ_2) of the weighted misfit to construct the likelihood function. The weights are designed to selectively fit different portions of the time series. For the ℓ_2 norm, we use a Gaussian likelihood and for the ℓ_1 norm we use a symmetric Laplace likelihood. While fitting the slip data, the mismatch between the computed and observed time-of-onset of slip at the borehole is used as an additional constraint. This is implemented by including in the misfit norm (positive real number) penalties imposed at each such instant of observed slip where the model predicts no slip at the borehole. These penalties are derived such that they are all equal across a particular modeled slip time series and add up to the total data misfit norm. Typically, we discarded a significant initial portion (around 25%) of the Markov chain as burn-in and only retained the converged chain for analysis.

Inverting for hydrological parameters

The pore pressure build-up at the well, in response to the time variable volume injection rate (gray curve in Figure 2A), is recorded at 1 Hz (black curve in Figure 2A). The time-history of pore pressure shows multiple instances where the pressure head drops anomalously even though the imposed injection rate remained non-decreasing. Our pore pressure diffusion model, with constant k and M, cannot accommodate such data. In particular, when fitting across these large, anomalous drops in pore pressure, we found that assuming a constant layer permeability (k) for the whole observed pore-pressure time series produced a good fit to either the time-history before or after the pressure drops around $t_{\text{break}} \sim 620$ s. Additionally, the Biot modulus (M) was estimated at $\sim 10^5$ GPa from these inversions, which is unrealistic.

The simplest modification to this problem is to add a step change in permeability around 620 s (we used 618 s) and, thus, add a second permeability to the model – k is k_1 for $t \leq 618$ s and k_2 for $t > 618$ s. This 3-parameter model (blue curve in Figure 2A and posteriors in B-C) produced much improved fits to the data even though, for the best fitting model, k_2 was found to be only 20% larger than k_1. However, the best fitting 3-parameter model still required an unrealistic $M \sim 10^5$ GPa.

We resolved this problem by introducing a second step-change in permeability to capture the pressure drop around 940 s. In this 4-parameter model (k_1, k_2, k_3 and M), we had $k = k_2$ for 618 s $\leq t <$ 940 s. and $k = k_3$ for $t \geq$ 940 s. This 4-parameter model (minimum root-mean-square error fit shown as red curve in Figure 2A and posteriors in Figures 2D-E) produces a better fit to the pressure time series with reasonable values of M. Moreover, the storativity corresponding to this estimated value of M ($\sim$ 50 MPa) and the damage zone width noted by *Guglielmi et al.* (2015a) ($\sim$ 0.2 m) lie within the range of previously reported geological scale estimates from damage zones of active faults ($10^{-4} - 10^{-5}$) (*Doan et al.*, 2006; *Xue et al.*, 2013). The permeabilities derived from this model are also consistent with estimates from previous pulse injection tests carried out in the test area (10^{-12} m^2) (*Jeanne et al.*, 2013). We choose the set of 4 parameters yielding the minimum root-mean-square error (MRMSE) of the model as the appropriate description for the spatio-temporal pore pressure evolution that drives the shear rupture. The hydrologic model with this parameter set has a hydraulic diffusivity of around 4×10^{-2} m^2/s.

In the 4-parameter hydrological model (Figure 2D), it is notable that the permeabilities bear the relationship $k_3 > k_2 > k_1$ with a cumulative 60% enhancement in permeability. The permeability of fault damage zones has been observed to vary in response to pore-pressure (*Seront et al.*, 1998; *Scuderi and Collettini*, 2016), dynamic stresses induced by wave-propagation (*Xue et al.*, 2016; *Elkhoury et al.*, 2006), near-field co-seismic static stresses (*Muir-Wood and King*, 1993; *Wang et al.*, 2016) and with accumulating shear slip both on reactivated faults in the laboratory (*Gutierrez et al.*, 2000; *Wu et al.*, 2017; *Im et al.*, 2018) and *in situ* on pre-existing faults (*Guglielmi et al.*, 2015a,b). In particular, the role of shear-induced dilation to increase porosity (*Jeanne et al.*, 2018) or the hydraulic aperture of fractures (*Guglielmi et al.*, 2015b; *Im et al.*, 2018) has been commonly cited as the mechanism behind permeability enhancement due to slip. Our estimates of the step changes in permeability indicate that permeability enhancement seems to saturate even as slip continues to accumulate at an accelerated rate (the posteriors for k_3 and k_2 overlap significantly more than those for k_1 and k_2 in Figure 2C). Interestingly, the measured accumulation of fault normal displacement in this experiment also saturates and remains largely insensitive to the accumulation of slip beyond approximately 1000 s. (*Guglielmi et al.*, 2015a). The concomitant saturation of permeability enhancement may point to the primacy of pressurization- or shear-induced dilation as the operative mechanism.

Inferring mechanical properties with a constant friction model

The *Guglielmi et al.* (2015a) data shows a modest acceleration of slip around 830 s. and a more marked acceleration of slip after around 1200 s of injection. Figure 3A shows fits to different portions of the observed slip at the borehole when the friction coefficient of the fault is assumed to be constant. These fits were derived using the pore-pressure diffusion model inferred from the minimum root-mean-square error 4-parameter fit to the hydrological data. Our model, with friction held constant at a level f and no time-dependent poroelastic perturbations to σ, fits the time history of slip prior to $t \sim 828$ s reasonably well (green dotted fit in Figure 3A) with realistic estimates for G_{out}/f and $T = 1 - \tau/f\sigma$. Assuming $f = 0.6$ (and $\sigma = 3.35$ MPa from *Guglielmi et al.* (2015a)), we get $G_{\text{out}} \sim 5.75$ GPa and $\tau \sim 2.75$ MPa from this fit. We note that this fit also predicts that the growth of the rupture radius $L(t)$ starts to outpace the growing pore-pressure diffusion front (the diffusive length scale is defined as the e-folding distance of the pore-pressure profile from its maximum at the injection well) around 1000 s.

When we include the full slip history across the first 1170 s. in the misfit calculation, the resultant MRMSE model (yellow dashed line in Figure 3A) produces a considerably worse fit

to the data than when fitting the first 828 s alone. Notably, the parameters inferred from both these fits appear pretty similar. However, it is clear that even the modest acceleration in slip between 828 s and 1170 s cannot be fit by this constant friction model.

To fit the more dramatic accelerated slip accumulation observed beyond the first 1170 s of injection we do not penalize the slip onset anymore. We find that a reasonable fit to this portion of the slip time history (solid red line in Figure 3A) comes at the expense of (i) the misprediction of the onset time as around 820 s, (ii) an extremely poor fit to the slip history between 828 s and 1170 s of injection including a period of back-slip owed to model limitations, and (iii) unreasonably small values of the shear modulus G_o ($\sim$ 31.9 MPa assuming $f = 0.6$) of the intact rock bounding the fault core.

Modeling accelerating slip with a variable friction model

In the absence of time-dependent poro-elastic strains, and with a constant friction coefficient, the spatio-temporal history of pore-pressure is the only source of variation in fault strength in our model. Given the injection time history, and a good fit to the observed pore-pressure time series, it is clear that such a model is incapable of reproducing the transient accelerations in slip observed in the data of *Guglielmi et al.* (2015a). One possible modification to this model would be to include variations in the friction coefficient with slip or slip rate. While there is evidence for both slip-weakening (*Wawersik and Fairhurst*, 1970; *Wawersik and Brace*, 1971; *Wong*, 1982) and rate (and slip) dependence (*Dieterich*, 1972; *Ruina*, 1983; *Marone*, 1998; *Beeler et al.*, 1994) from laboratory friction experiments, we attempt to fit the slip data, instead, with a simplified proxy for the more complicated, genuine slip- or rate-dependence as a first pass. We assume that the friction coefficient undergoes step changes everywhere on the fault at certain chosen times much like the damage zone permeability. When no a priori relationship between these friction levels are assumed, the inter-relationships between the inferred friction levels is expected to contain unbiased information about whether true slip- and/or rate-dependence in the friction coefficient can produce better fits to the slip time series, while allowing us to use the same numerical framework as the constant friction fits of the previous section.

In Figure 3B we show preliminary inversion results under this piecewise constant friction model (Figure 4A). Though these results were not derived from robust, steady-state, Monte Carlo chains as the fits in Figures 2 and 4, these initial results show that the imposed variations in friction lead to a significantly better fit to the slip time history. By trial-and-error, we found that a good visual fit to the data requires a minimum of 4-5 step changes in friction at the times indicated in by the vertical dashed lines in Figure 4A. The resultant time-history of friction reveals support for both slip- and rate-dependence. To see this, note that the first 3 step-changes in friction correspond to modest to large changes in the slip rate at the borehole while the last 2 correspond to continued slip accumulation at what appears to be an accelerated but constant rate. Therefore, the reduction of friction across the first 3 step-changes seem more consistent with rate-weakening at the borehole while the reduction across the last 2 seem more consistent with continued slip-weakening.

While this piecewise constant model of variation in the frictional strength is entirely contrived, this first-pass inversion suggests that a friction model that contains both rate- and slip-dependence would do a considerably better job of fitting the observed slip time-history than the constant friction model. This in turn suggests that laboratory-derived rate-state constitutive relations for sliding friction (*Dieterich*, 1972; *Ruina*, 1983), which naturally combine both rate- and slip-dependence, might also do better than models which incorporate either slip- or rate-dependence alone. In this sense, even this preliminary analysis points towards the relevance

of laboratory-derived friction constitutive relations in capturing 'real' fault behavior in nature and suggests the usefulness of such experimental data in bridging the laboratory and field scale gap.

Conclusions

This report contains work carried out within the funding period of the USGS EHP grant No. G17AP00016. The proposal had laid out plans for studying elementary models in which fluid flow in the focused damage zone of a fault induces aseismic slip and comparing these models with *in situ* observations from the field-scale fluid injection experiments of *Guglielmi et al.* (2015a). We completed work on this proposed problem within two broad areas – (i) building numerical models for axi-symmetric pore-pressure diffusion within a fault damage zone in response to fluid-injection and the resultant evolution of fault-slip within a quasi-circular rupture, and (ii) comparing the model results to the *Guglielmi et al.* (2015a) dataset within a Bayesian inversion framework. Our modeling and inversion results reveal that the observations of fluid-activated aseismic slip in the experiments of *Guglielmi et al.* (2015a) provide evidence for the evolution of both hydraulic and mechanical parameters of the fault and damage zone complex with continued injection and activated slip. In particular, we find that the observed pore-pressure time history requires permeability enhancement with accumulating pore-pressure and slip while the observed slip time-history requires the friction coefficient to vary with slip and/or slip rate. This work, to our knowledge, represents one of the first steps towards assimilating direct observational constraints from the behavior of faults in nature into numerical models of fault slip. We envision this unique data driven approach to fault mechanics as being an important bridge between our understanding of fault mechanics at the lab scale and the field scale.

References

Beeler, N. M. (2007), Laboratory-observed faulting in intrinsically and apparently weak materials, in *The Seismogenic Zone of Subduction Thrust Faults*, edited by T. Dixon and C. Moore, chap. 13, pp. 370–449, Columbia Univ. Press, New York, doi:10.7312/dixo13866.

Beeler, N. M., T. E. Tullis, and J. D. Weeks (1994), The roles of time and displacement in the evolution effect in rock friction, *Geophysical Research Letters*, *21*, 1987–1990.

Bhattacharya, P., A. M. Rubin, E. Bayart, H. M. Savage, and C. Marone (2015), Critical evaluation of state evolution laws in rate and state friction: Fitting large velocity steps in simulated fault gouge with time-, slip-, and stress-dependent constitutive laws, *Journal of Geophysical Research: Solid Earth*, *120*(9), 6365–6385, doi:10.1002/2015JB012437.

Bouchon, M., V. Durand, D. Marsan, H. Karabulut, and J. Schmittbuhl (2013), The long precursory phase of most large interplate earthquakes, *Nature Geoscience*, *6*, 299–302, doi:10.1038/ngeo1770.

Charléty, J., N. Cuenot, L. Dorbath, C. Dorbath, H. Haessler, and M. Frogneux (2007), Large earthquakes during hydraulic stimulations at the geothermal site of Soultz-sous-Forêts, *International Journal of Rock Mechanics and Mining Sciences*, *44*(8), 1091–1105, doi:10.1016/j.ijrmms.2007.06.003.

Cornet, F. H. (2016), Seismic and aseismic motions generated by fluid injections, *Geomechanics for Energy and the Environment*, *5*, 42–54, doi:10.1016/j.gete.2015.12.003.

Cornet, F. H., J. Helm, H. Poitrenaud, and A. Etchecopar (1997), Seismic and aseismic slips induced by large-scale fluid injections, *Pure and Applied Geophysics*, *150*(3), 563–583, doi:10.1007/s000240050093.

Coyle, B. J., and M. D. Zoback (1988), In situ permeability and fluid pressure measurements at $\sim$2 km depth in the Cajon Pass research well, *Geophysical Research Letters*, *15*(9), 1029–1032, doi:10.1029/GL015i009p01029.

Deichmann, N., and D. Giardini (2009), Earthquakes induced by the stimulation of an enhanced geothermal system below Basel (Switzerland), *Seismological Research Letters*, *80*(5), 784–798, doi:10.1785/gssrl.80.5.784.

Detournay, E., and A. H.-D. Cheng (1993), Fundamentals of poroelasticity, in *Analysis and Design Methods*, edited by C. Fairhurst, pp. 113–171, Pergamon, Oxford, doi:10.1016/B978-0-08-040615-2.50011-3.

Dieterich, J. H. (1972), Time-Dependent Friction in Rocks, *Journal of Geophysical Research*, *77*(20), 3690–3697, doi:10.1029/JB077i020p03690.

Doan, M. L., E. E. Brodsky, Y. Kano, and K. F. Ma (2006), In situ measurement of the hydraulic diffusivity of the active Chelunepu Fault, Taiwan, *Geophysical Research Letters*, *33*, L16317, doi:10.1029/2006GL026889.

Dodge, D. A., G. C. Beroza, and W. L. Ellsworth (1996), Detailed observations of {C}alifornia foreshock sequences: Implications for the earthquake initiation process, *J. Geophys. Res.: Solid Earth*, *101*(B10), 22,371–22,392, doi:10.1029/96JB02269.

Elkhoury, J. E., E. E. Brodsky, and D. C. Agnew (2006), Seismic waves increase permeability, *Nature*, *441*, 1135–1138, doi:10.1038/nature04798.

Ellsworth, W. L. (2013), Injection-Induced Earthquakes, *Science*, *341*(6142), 1225942., doi:10.1126/science.1225942.

Gao, H. (1988), Nearly circular shear mode cracks, *International Journal of Solids and Structures*, *24*(2), 177–193, doi:https://doi.org/10.1016/0020-7683(88)90028-5.

Garagash, D. I., and L. N. Germanovich (2012), Nucleation and arrest of dynamic slip on a pressurized fault, *Journal of Geophysical Research: Solid Earth*, *117*, B10310, doi:10.1029/2012JB009209.

Guglielmi, Y., F. Cappa, J. P. Avouac, P. Henry, and D. Elsworth (2015a), Seismicity triggered by fluid injection-induced aseismic slip, *Science*, *348*(6240), 1224–1226, doi:10.1126/science.aab0476.

Guglielmi, Y., D. Elsworth, F. Cappa, P. Henry, C. Gout, P. Dick, and J. Durand (2015b), In situ observations on the coupling between hydraulic diffusivity and displacements during fault reactivation in shales, *Journal of Geophysical Research: Solid Earth*, *120*(11), 7729–7748, doi:10.1002/2015JB012158.

Gutierrez, M., L. E. Øino, and R. Nygård (2000), Stress-dependent permeability of a demineralised fracture in shale, *Marine and Petroleum Geology*, *17*(8), 895–907, doi:10.1016/S0264-8172(00)00027-1.

Hastings, W. K. (1970), Monte Carlo sampling methods using Markov chains and their applications, *Biometrika*, *57*(1), 97–109, doi:10.2307/2334940.

Hubbert, M. K., and W. W. Rubey (1959), Role of fluid pressure in mechanics of overthrust faulting, *Geological Society of America Bulletin*, *70*(2), 115–166, doi:10.1130/0016-7606(1959)70[115:rofpim]2.0.co;2.

Im, K., D. Elsworth, and Y. Fang (2018), The influence of preslip sealing on the permeability evolution of fractures and faults, *Geophysical Research Letters*, *45*(1), 166–175, doi:10.1002/2017gl076216.

Jeanne, P., Y. Guglielmi, and F. Cappa (2013), Dissimilar properties within a carbonate-reservoir's small fault zone, and their impact on the pressurization and leakage associated with CO2injection, *Journal of Structural Geology*, *47*(Supplement C), 25–35, doi:10.1016/j.jsg.2012.10.010.

Jeanne, P., Y. Guglielmi, J. Rutqvist, C. Nussbaum, and J. Birkholzer (2018), Permeability variations associated with fault reactivation in a claystone formation investigated by field experiments and numerical simulations, *Journal of Geophysical Research: Solid Earth*, *123*(2), 1694–1710, doi:10.1002/2017JB015149.

Keranen, K. M., M. Weingarten, G. A. Abers, B. A. Bekins, and S. Ge (2014), Sharp increase in central Oklahoma seismicity since 2008 induced by massive wastewater injection, *Science*, *345*(6195), 448–451, doi:10.1126/science.1255802.

Marone, C. (1998), Laboratory derived fricition laws and their application to seismic faulting, *Annual Review of Earth Planetary Science*, *26*, 643–696, doi:10.1146/annurev.earth.26.1.643.

Marone, C., and D. M. Saffer (2015), The Mechanics of Frictional Healing and Slip Instability During the Seismic Cycle, in *Treatise on Geophysics (Second Edition)*, edited by G. Schubert, second edi ed., pp. 111–138, Elsevier, Oxford, doi:https://doi.org/10.1016/B978-0-444-53802-4.00092-0.

Metropolis, N., A. W. Rosenbluth, M. N. Rosenbluth, A. H. Teller, and E. Teller (1953), Equation of State Calculations by Fast Computing Machines, *Journal of Chemical Physics*, *21*, 1087–1092, doi:10.1063/1.1699114.

Muir-Wood, R., and G. C. P. King (1993), Hydrological signatures of earthquake strain, *Journal of Geophysical Research: Solid Earth*, *98*(B12), 22,035–22,068, doi:10.1029/93JB02219.

Raleigh, C. B., J. H. Healy, and J. D. Bredehoeft (1976), An Experiment in Earthquake Control at Rangely, Colorado, *Science*, *191*(4233), 1230–1237, doi:10.1126/science.191.4233.1230.

Ruina, A. (1983), Slip instability and state variable friction laws, *Journal of Geophysical Research*, *88*, 10,359–10,370, doi:10.1029/JB088iB12p10359.

Salamon, N. J., and J. Dundurs (1971), Elastic fields of a dislocation loop in a two-phase material, *Journal of Elasticity*, *1*(2), 153–164, doi:10.1007/BF00046466.

Salamon, N. J., and J. Dundurs (1977), A circular glide dislocation loop in a two-phase material, *Journal of Physics C: Solid State Physics*, *10*(4), 497–507, doi:10.1088/0022-3719/10/4/007.

Scotti, O., and F. H. Cornet (1994), In Situ Evidence for fluid-induced aseismic slip events along fault zones, *International Journal of Rock Mechanics and Mining Sciences and Geomechanics*, *31*(4), 347–358, doi:10.1016/0148-9062(94)90902-4.

Scuderi, M. M., and C. Collettini (2016), The role of fluid pressure in induced vs. triggered seismicity: Insights from rock deformation experiments on carbonates, *Scientific Reports*, 6, 24852, doi:10.1038/srep24852.

Seront, B., T. F. Wong, J. S. Caine, C. B. Forster, R. L. Bruhn, and J. T. Fredrich (1998), Laboratory characterization of hydromechanical properties of a seismogenic normal fault system, *Journal of Structural Geology*, doi:10.1016/S0191-8141(98)00023-6.

Shapiro, S. A., E. Huenges, and G. Borm (1997), Estimating the crust permeability from fluid-injection-induced seismic emission at the KTB site, *Geophysical Journal International*, *131*(2), F15–F18, doi:10.1111/j.1365-246X.1997.tb01215.x.

Shapiro, S. A., E. Rothert, V. Rath, and J. Rindschwentner (2002), Characterization of fluid transport properties of reservoirs using induced microseismicity, *Geophysics*, *67*(1), 212–220, doi:10.1190/1.1451597.

Townend, J., and M. D. Zoback (2000), How faulting keeps the crust strong, *Geology*, *28*(5), 399–402, doi:10.1130/0091-7613(2000)28⟨399:HFKTCS⟩2.0.CO;2.

Wang, C.-Y., X. Liao, L.-P. Wang, C.-H. Wang, and M. Manga (2016), Large earthquakes create vertical permeability by breaching aquitards, *Water Resources Research*, *52*(8), 5923–5937, doi:10.1002/2016wr018893.

Wawersik, W. R., and W. F. Brace (1971), Post-failure behavior of a granite and diabase, *Rock Mechanics Felsmechanik Mécanique des Roches*, doi:10.1007/BF01239627.

Wawersik, W. R., and C. Fairhurst (1970), A study of brittle rock fracture in laboratory compression experiments, *International Journal of Rock Mechanics and Mining Sciences and Geomechanics*, doi:10.1016/0148-9062(70)90007-0.

Wei, S., et al. (2015), The 2012 Brawley swarm triggered by injection-induced aseismic slip, *Earth and Planetary Science Letters*, *422*, 115–125, doi:10.1016/j.epsl.2015.03.054.

Weingarten, M., S. Ge, J. W. Godt, B. A. Bekins, and J. L. Rubinstein (2015), High-rate injection is associated with the increase in U.S. mid-continent seismicity, *Science*, *348*(6241), 1336–1340, doi:10.1126/science.aab1345.

Wong, T.-F. (1982), Shear fracture energy of Westerly granite from post-failure behavior, *Journal of Geophysical Research*, 87(B2), 990–1000, doi:10.1029/JB087iB02p00990.

Wu, W., J. S. Reece, Y. Gensterblum, and M. D. Zoback (2017), Permeability Evolution of Slowly Slipping Faults in Shale Reservoirs, *Geophysical Research Letters*, *44*(22), 11,368–11,375, doi:10.1002/2017GL075506.

Xue, L., et al. (2013), Continuous permeability measurements record healing inside the Wenchuan earthquake fault zone, *Science*, *340*(6140), 1555–1559, doi:10.1126/science.1237237.

Xue, L., E. E. Brodsky, J. Erskine, P. M. Fulton, and R. Carter (2016), A permeability and compliance contrast measured hydrogeologically on the San Andreas Fault, *Geochemistry, Geophysics, Geosystems*, doi:10.1002/2015GC006167.

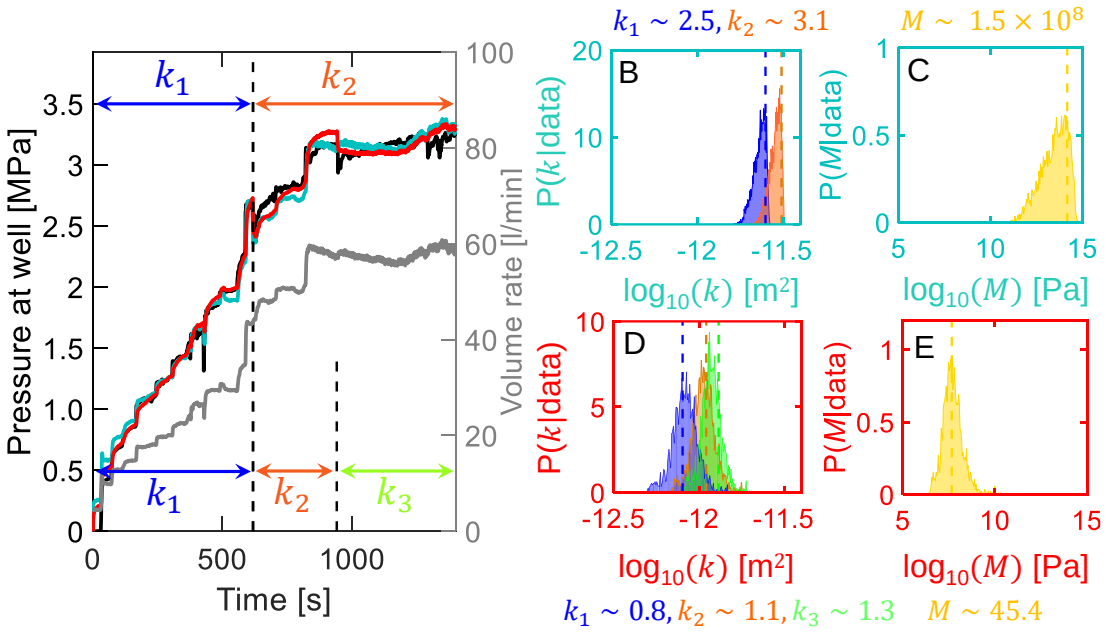

Figure 2: Fits to the observed pore-pressure history at the well. (A) Comparing the 3-parameter hydrological fit (blue curve, 1 step change in k, constant M) to the 4-parameter hydrological fit (red curve, 2 step changes in k, constant M). The observed pore pressure data is shown in black. Both models fit the observations closely while only the 4-parameter model yields realistic values for both permeability and storage coefficients. The imposed injection rate time series is shown in gray. For the 3- and 4-parameter models, permeability k_1 changes to k_2 at 618 s; k_2 is subsequently updated to k_3 at 940 s for the 4-parameter hydrological model. (B)-(C) Posteriors for k_1 (red area plot), k_2 (blue area plot) and M (yellow area plot) respectively for the 3-parameter fit. (D)-(E) Posteriors for k_1 (red area plot), k_2 (blue area plot), k_3 (green area plot) and M (yellow area plot) for the 4-parameter fit. The vertical dashed lines show the minimum root-mean-square error (MRMSE) estimates from the MCMC sampled posteriors. The numbers in color correspond to these MRMSE estimates. The permeability numbers are in 10^{-12} m^2, the values of the Biot modulus in MPa.

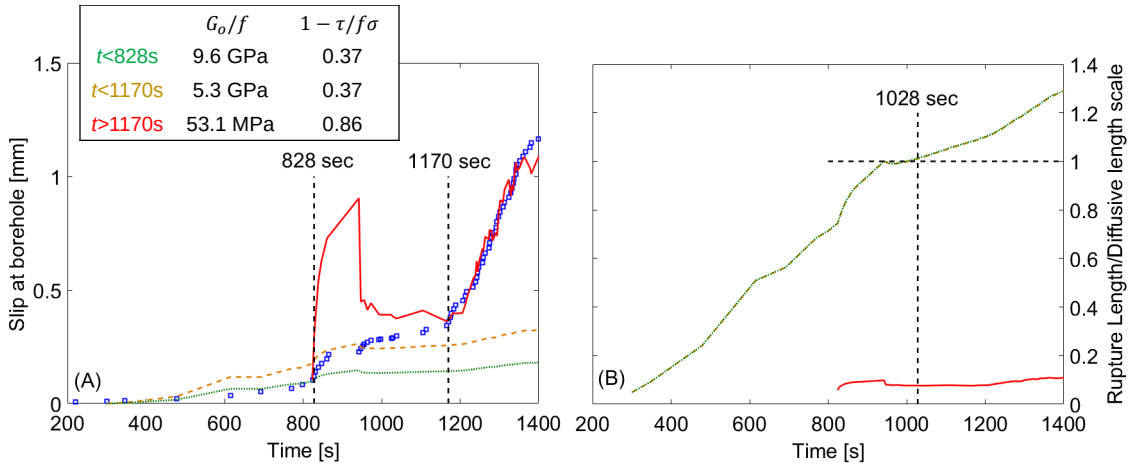

Figure 3: Constant friction fits to the time history of slip observed at the borehole with the spatio-temporal distribution of pore-pressure derived from the MRMSE fit to the observed pore-pressure time history. (A) Fits to various portions of the observed slip time series (blue squares). Green dotted line is the best fit to the slip data prior to 828 s. and the yellow dashed line is the best fit to observed slip for $t < 1170$ s. The red solid curve shows the fit to the slip history for $t > 1170$ s. Except for this last fit (for $t > 1170$ s), all other fits are constrained to match both the time-variations in slip and its onset. Note, that the fit to the slip time history for $t > 1170$ s produces a significantly worse fit to the slip history in the preceding time interval and predicts the onset of slip around 820 s. This fit also requires the undamaged host rock to be unreasonably compliant – the shear modulus G_o is estimated to be 31.9 MPa assuming $f = 0.6$. (B) The corresponding time evolutions of the ratio of rupture length $L(t)$ to a diffusive length scale. The diffusive length scale is defined as the e-folding distance of the pore-pressure profile from its maximum at the borehole. Note that the fits to the slip history which are constrained to match the onset time of slip (those fitting data at times only before $t < 1170$ s.) both return identical values of the parameter $1 - \tau/f\sigma$ and lead to identical time evolutions of rupture length. This is because, similar to the 1D case, $1 - \tau/f\sigma$ controls the rupture length for the constant friction crack for 2D ruptures for a specified pore-pressure history. These fits also show that the slipping region starts to outpace pore-pressure diffusion around 1028 s.

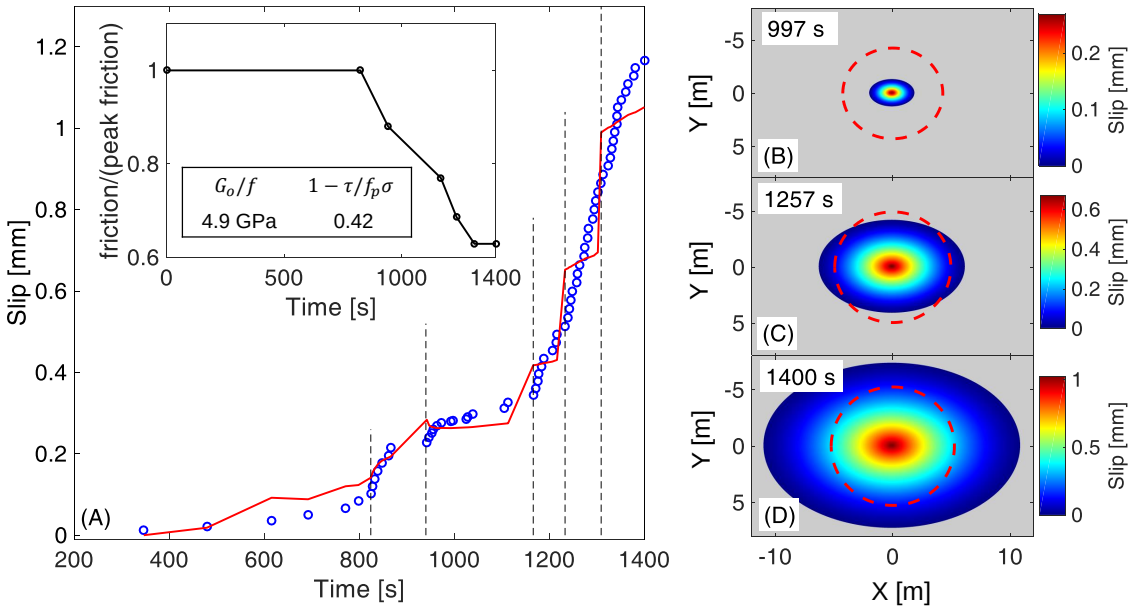

Figure 4: (A) Fit to the slip history with a piecewise constant friction coefficient which varies with continued accumulation of slip. Unlike true slip- or rate-dependence, the friction coefficient is assumed to undergo step-changes everywhere in space at chosen times much like the permeability model in Figure 2. The times for these step-changes (shown by the dashed vertical lines) were chosen by trial-and-error to minimize RMSE and produce a good visual fit to the data. Inset shows the inferred time-history of friction. (B)-(D) shows the extent of the rupture at three time snapshots that the resultant rupture front outpaces pore-pressure diffusion. Red dashed contours show 0.5 MPa increase in pore-pressure.